stellarator news

Published by Fusion Energy Division, Oak Ridge National Laboratory
Building 5700 P.O. Box 2008 Oak Ridge, TN 37831-6169, USA

Editor: James A. Rome Issue 97 March 2005
E-Mail: jar@ornl.gov Phone (865) 482-5643
On the Web at *http://www.ornl.gov/sci/fed/stelnews*

Columbia Non-neutral Torus completes construction and starts operation

The Columbia Non-neutral Torus (CNT), located at Columbia University in New York City, is a simple, relatively small stellarator designed to study confinement of non-neutral and electron-positron plasmas confined on magnetic surfaces. CNT started operation in November 2004. Our initial results include a detailed mapping of the magnetic surfaces, development of ways to visualize the magnetic surfaces in three dimensions, and attainment of the ultrahigh-vacuum range with internal coils.

Basic configuration

CNT has a very simple coil system with only two pairs of circular coils [1, 2]. Thus, the magnet system of CNT is simpler than that of any other stellarator — indeed, simpler than that of any tokamak. As shown in Fig. 1, two of the coils are interlocked and are placed inside the vacuum chamber. Each of the interlocked coils is encased in its own stainless steel vacuum case, with atmospheric

In this issue . . .

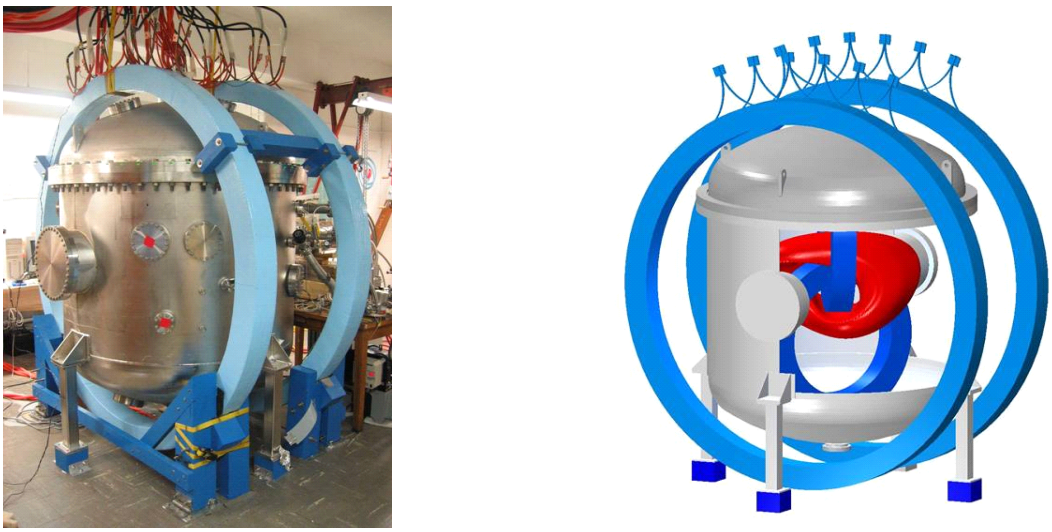

Fig. 1. Left: CNT in the Columbia Plasma Physics Laboratory. Right: CAD drawing giving a partial view of the four coils and the shape of the last closed flux surface inside the vacuum chamber.

pressure on the inside and ultrahigh vacuum on the outside, and with the leads brought out through a custom ultrahigh-vacuum feedthrough. The angle between these two coils can be adjusted from 64° to 88°, allowing the creation of substantially different stellarator configurations. Our present configuration is at 64°, which is characterized by an extremely low aspect ratio (predicted to be 1.8) and a modest iota with some shear (ι = 0.11 on axis and 0.22 at the plasma edge). At 88°, the aspect ratio is approximately 2.5, and ι is 0.56.

Design and construction phase

Funding for CNT construction and operation was secured in the form of a Plasma Physics Junior Faculty Grant from the U.S. Department of Energy (DOE) starting in September 2002, and a National Science Foundation (NSF)/DOE grant was secured for the theoretical and numerical research in August 2003. The design was done jointly by Columbia University (Pedersen, Kremer) and Princeton Plasma Physics Laboratory (PPPL; Dahlgren, Reiersen, Pomphrey). The vacuum chamber was built by Ability Engineering, South Holland, Illinois, and delivered in June 2004. The two large external coils, which are standard water-cooled copper coils, were the first two production coils from the small company AMP Electric Machines, of Mertztown, Pennsylvania. They were also delivered in June 2004. The interlocked, stainless steel encased coils were built by Alpha Magnetics, Hayward, California, and delivered in October 2004. A special winding table had to be assembled around the first coil to allow winding of the second coil interlocked with the first one. The setup is shown in Fig. 2. The two coils were installed in the CNT vacuum chamber in November 2004.

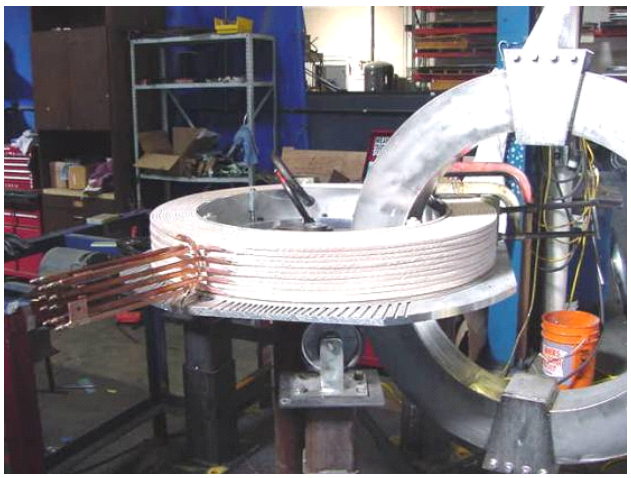

Fig. 2. The second internal coil at Alpha Magnetics after completion of winding, interlocked with the first internal coil.

Field line mapping results

The magnetic surface structure in CNT has been mapped out for the 64° angle configuration. The aspect ratio A is very low (a preliminary analysis confirms $A < 2$) with no significant island chains in the interior, as shown in Fig. 3. The field line mapping was done using a 50-eV electron beam (e-beam) emitted from a small movable electron gun. The e-beam was intersected by two ZnO-coated aluminum rods that emit light when struck by the e-beam. The two rods were rotated through each magnetic surface, allowing a standard digital camera to record an entire magnetic surface in a 5-s exposure taken through a quartz window on the vacuum chamber. Multiple photos were then manipulated and combined using IDL software to create the composite image in Fig. 3. The last good magnetic surface is surrounded by a 2/9 island chain, as predicted by numerical calculations. This island chain is barely visible in Fig. 3.

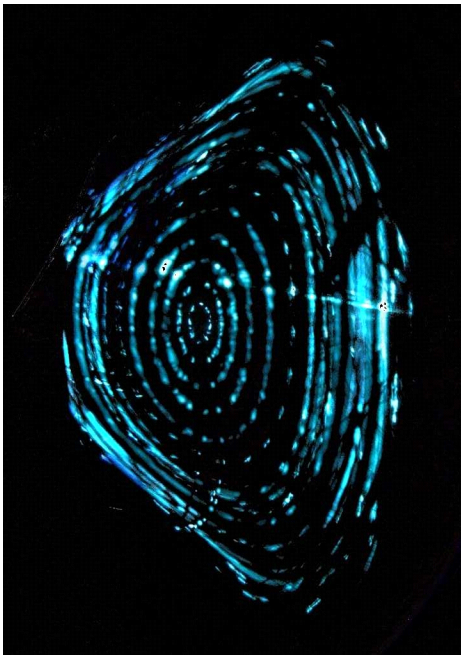

Fig. 3. Nested magnetic surfaces in CNT, mapped out using an electron beam and two rotatable ZnO-coated rods.

Field line mapping was done at 0.08 T and at pressures in the 10^{-8} Torr range. At this rather low field (CNT can be run up to 0.33 T), the magnets can be pulsed for minutes at a time, greatly facilitating field line mapping. These results are being analyzed in detail and written up for publication in a peer-reviewed journal.

Three-dimensional visualization of the magnetic field

The magnetic surfaces were visualized in three dimensions using the e-beam and a backfill of neutral gas. The e-beam excites and ionizes the background neutral gas, which then radiates visible light, allowing one to see the field lines and even whole magnetic surfaces. If the neutral pressure

is not too high, the e-beam spreads out only slowly and is therefore approximately tied to the magnetic surface on which it was injected. The most striking visualizations of surfaces (and single field lines) were obtained with an e-beam energy of approximately 200 eV and a neutral gas fill of air at a pressure of 5×10^{-5} Torr. Other gases, such as helium and argon, were also used but did not produce as much light. An example of a glowing magnetic surface, photographed by a standard digital camera through a quartz viewport, is shown in Fig. 4.

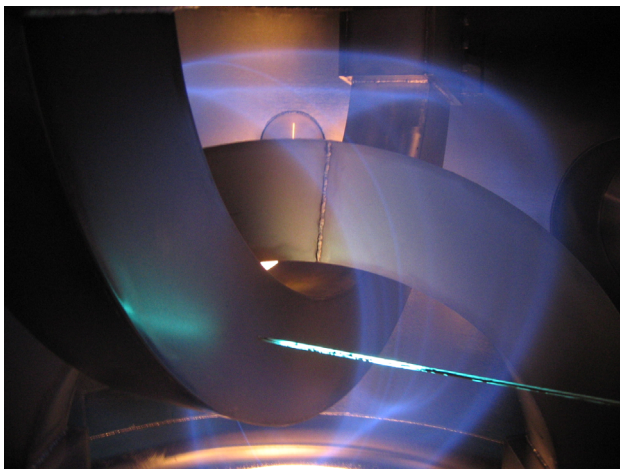

Fig. 4. A glowing magnetic surface created by collisions between an electron beam and air at 5×10^{-5} Torr. One of the phosphorescent rods is visible, lit up by electrons.

Plans for the immediate future

The next phase for CNT involves creation and studies of the first pure electron plasmas. Although the hot filament discharges created to visualize magnetic surfaces were plasmas, they were quasi-neutral and hence not of the kind to be studied in CNT. Creation of pure electron plasmas requires significant injection of low-energy electrons in an ultrahigh vacuum (~10^{-9} Torr). This vacuum level has been achieved. Movable electron emitters and diagnostic probes are under construction. The electron emitters differ from the electron gun by having a much larger spatial extent, in order to fill many magnetic surfaces with low-energy electrons. Each emitting filament will be independently biased to help tailor the electrostatic potential profile, which will affect the density profile.

Background: Some basic physics to be explored in CNT

The non-neutral plasmas in CNT will exhibit new physics; the low-density equilibrium for a pure electron plasma is governed by a Poisson-Boltzmann equation for the electrostatic potential [3,4]:

$$\frac{\varepsilon_0}{e}\nabla^2\phi = N(\psi)e^{e\phi/T_e(\psi)}$$

Here, ψ is the coordinate that describes the magnetic surfaces. This equation is unlike either that describing neutral plasmas in stellarators, or that describing non-neutral plasmas in previously studied configurations, such as Penning traps. Confinement in a non-neutral stellarator plasma is predicted to be excellent, because the strong $\boldsymbol{E} \times \boldsymbol{B}$ drift created by the space charge acts as an effective rotational transform. Since CNT will be operating with a deficit of ions, it is operating in some sense in the ion root. However, because of the complete lack of ions and the significant number of electron Debye lengths, we can study particle confinement in the extreme limit of $|e\phi/T| >> 1$, where confinement times could be seconds or even minutes [3,5]. Considering that CNT is a classical stellarator, not optimized for neoclassical confinement, this would be a significant demonstration of the beneficial effects of strong electric fields on confinement in stellarators.

If such long confinement times can be achieved, then CNT can be used to create the first laboratory electron-positron plasma. Electron-positron plasmas are unique and simple because of the electron-positron symmetry. For example, acoustic waves and drift waves are absent in these plasmas. Despite their unique properties, such plasmas have not yet been created in a laboratory, because existing sources of positrons are weak; a confinement device that has extremely long confinement times and yet can confine both negative and positive particles simultaneously is needed. Penning traps, for instance, can confine positrons for weeks, but are unable to confine both positive and negative species simultaneously. Magnetic surface configurations can confine both positive and negative charges, but confinement times are limited by turbulence and neoclassical transport. However, if a strongly negative plasma, such as an initially pure electron plasma, can be confined for minutes in a stellarator, it can be used to accumulate significant amounts of positrons, hence allowing electron-positron plasmas to be created and studied [6].

References

[1] T. Sunn Pedersen, A.H. Boozer, J. P. Kremer, R. Lefrancois, F. Dahlgren, N. Pomphrey, W. Reiersen, W. Dorland, The Columbia Non-neutral Torus: A new experiment to confine non-neutral and positron-electron plasmas in a stellarator, Fusion Sci. and Technol. **46** p. 200

[2] C. Gourdon, D. Marty, E. K. Maschke, and J. P. Dumont, in Plasma Physics and Controlled Nuclear Fusion Research, p. 849, International Atomic Energy Agency, Vienna, Austria (1969).

[3] Thomas Sunn Pedersen and Allen H. Boozer, Confinement of nonneutral plasmas on magnetic surfaces, Phys. Rev. Lett. **88**, 205002 (2002).

[4] T. Sunn Pedersen, Numerical investigation of two-dimensional pure electron plasma equilibria on magnetic surfaces, Phys. Plasmas **10**, 334 (2003)

[5] T. Sunn Pedersen, Large electric fields in stellarators, in

Progress in Nuclear Fusion Research (Nova Science Publishers, in press).

[6] T. Sunn Pedersen, A. H. Boozer, W. Dorland, J. P. Kremer, and R. Schmitt, Prospects for the creation of positron-electron plasmas in a non-neutral stellarator, J. Phys. B **36**, 1029 (2003)

Thomas Sunn Pedersen
On behalf of the CNT Team
Dept. of Applied Physics and Applied Mathematics
Columbia University
New York, NY 10027, USA

E-mail: tsp22@columbia.edu
CNT Web site: http://www.ap.columbia.edu/CNT

Overview of confinement and MHD stability in the Large Helical Device

The Large Helical Device (LHD) is a superconducting heliotron device (poloidal period number $L = 2$, toroidal period number $M = 10$) with a major radius of $R_{ax} = 3.5$–4.1 m, an average minor radius of 0.6 m, and a magnetic field up to 3 T. LHD uses neutral beam heating (using negative ions with a beam energy of 150–180 keV with a radius of tangency R_{T_NBI} of 3.65–3.7 m).

Significant progress has been made in extending the plasma operational regime in various plasma parameters using neutral beam injection (NBI) with a power of 13 MW and electron cyclotron heating (ECH) with a power of 2 MW. The electron and ion temperatures have both reached 10 keV in the collisionless regime and the maximum electron density, the volume-averaged beta value, and stored energy are $2.4 \times 10^{20} m^{-3}$, 4.3%, and 1.3 MJ, respectively. In the last two years, intensive studies of MHD stability, methods of accessing the high-beta regime, and methods of healing the magnetic islands have been conducted. Local island divertor (LID) experiments also have been done to control the edge plasma with the goal of improving confinement. Transient transport analysis was performed for plasmas with an internal transport barrier (ITB) and a magnetic island.

A high ion temperature plasma was obtained by adding impurities to the plasma to keep the power deposition to the ions reasonably high even at very low density. By injecting 680 kW of ion cyclotron radio-frequency heating (ICRH), ECH, and NBI power, the plasma was sustained for 1905 seconds without serious problems of impurities or recycling; the total energy injected to the plasma was 1.3 GJ.

High beta experiment

The high beta experiment is done in the inward-shifted configuration, where the confinement is good enough, and the beta limit is low enough, to study the beta limit in a heliotron device. The highest operational beta value has been expanded from 3.2% to 4.3% in the last two years by increasing the heating capability and exploring a new magnetic configuration with a higher aspect ratio, obtained by changing the pitch parameter of the helical coil, $\gamma = n/2 \cdot a/R$, from 1.254 to 1.20. This new configuration with higher aspect ratio is characterized by a smaller volume and smaller Shafranov shift (measured by a soft X-ray CCD camera with tangential view) than the standard configuration, as seen in Fig.1. Although the MHD stability properties are expected, according to ideal MHD theory, to be even worse in this configuration ($\gamma = 1.22$) than in the so-called standard configuration ($\gamma = 1.254$), the smaller shift is considered to contribute to the central deposition of the neutral beam and hence a reduction in direct loss of the beam by keeping the magnetic axis close to the tangential radius of the neutral beam at higher beta. The distances between R_{T_NBI} and the magnetic axis position at $\langle \beta_{dia} \rangle = 0$ are indicated by the shaded region in Fig.1.

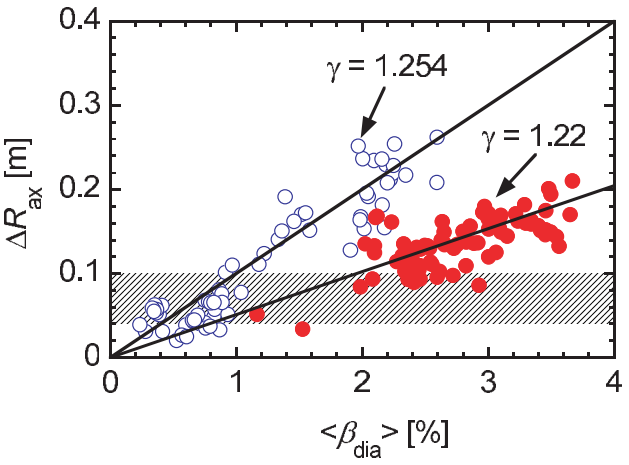

Fig.1. Shafranov shift of the magnetic axis ΔR_{ax} as a function of beta value for configurations with R_{ax} =3.6 and γ = 1.254 and 1.22.

The equilibrium reconstruction and stability analysis are performed for the high beta discharge using the 3-D MHD equilibrium code VMEC. Figure 2 shows the experimentally observed beta gradients at $\rho = 0.9$ in the configuration with $R_{ax} = 3.6$ m and $\gamma = 1.22$, where the rotational transform is estimated to be unity, as a function of $\langle \beta_{dia} \rangle$. The data were obtained in 0.45-T to 1.75-T operation. Here the gradients are evaluated with kinetic pressure measurements, and volume-averaged beta is given by diamagnetic loop measurements. The solid line in Fig. 2 denotes a contour of the low-n ($m/n = 1/1$) ideal MHD modes (with global mode structure) with $\gamma_{low\text{-}n}/\omega_A = 0.5 \times 10^{-2}$ and 1.0×10^{-2} for currentless equilibria. The growth rate is

calculated by a MHD stability analysis code (TERPSICHORE). Here $\omega_A = v_{A0}/R_0$, and v_{A0} and R_0 are the Alfvén velocity and the major radius at the magnetic axis. The dotted line is the stability boundary of Mercier modes (with a highly localized mode structure — high-m limit). The change of the gradients is observed around $\langle\beta_{dia}\rangle$ = 1.5%, which corresponds to the Mercier unstable region. However, the observed beta gradients at $\rho = 0.9$ increase with increasing beta up to $\langle\beta_{dia}\rangle = 4\%$. Here, the electron temperature profiles, measured with multi-channel YAG Thomson scattering, often show a local flattening at the rational surface, which is not included in the analysis using VMEC and Terpsichore.

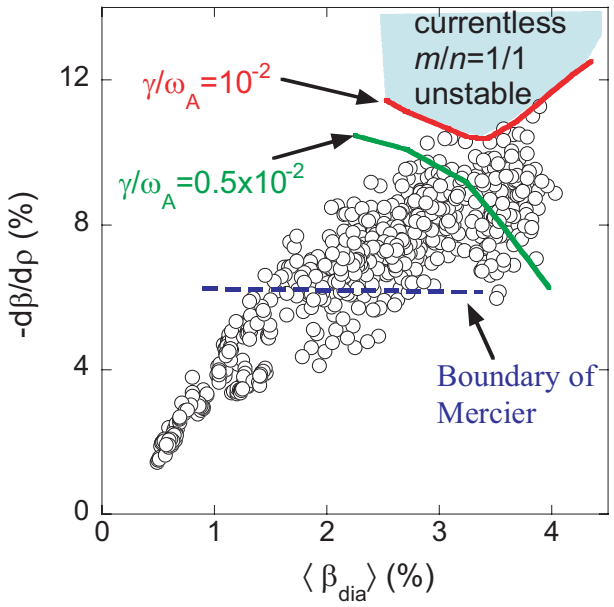

Fig. 2. Kinetic beta gradients at $\rho = 0.9$ ($\iota = 1$), $-d\beta/d\rho$ versus volume-averaged beta $\langle\beta\rangle$.

Local island divertor

In the LHD program, one of the key research goals is to enhance helical plasma performance through edge plasma control. For the first time in the LHD program, the edge plasma has been controlled using an LID. This is a closed divertor, utilizing an m/n = 1/1 island generated externally by 20 small perturbation coils. The LID head is inserted into the middle of the O-point of the island, so that the core plasma does not touch the divertor head. This prevents any leading edge problems. Since particle recycling is toroidally localized, the technical ease of hydrogen pumping is a big advantage of the LID over a closed full helical divertor. The LID experiment has been under way since 2002, and fundamental LID functions were demonstrated experimentally.

The outward heat and particle fluxes crossing the island separatrix flow along the field lines to the back side of the divertor head, where carbon plates are placed to receive the heat and particle loads. High-efficiency pumping is considered to be the key in realizing high-temperature divertor operation, resulting in an improvement of energy confinement.

In the helical divertor configuration, the energy confinement time depends on the position of the magnetic axis. The energy confinement time is higher than the prediction of ISS95 scaling by a factor of 1.5 in the configuration with R_{ax} = 3.6 m, while it is even slightly lower than the prediction of ISS95 scaling in the configuration with R_{ax} = 3.75 m. On the other hand, in the LID configuration, the energy confinement time is equal to or higher than the prediction of ISS95 scaling (1.2 times the scaling) even in the configuration with R_{ax} = 3.75 m. In the LID configuration, the energy transport at the edge region is clearly improved, as shown in Fig. 3. However, the main reason for the better confinement in the outward-shifted configuration appears to be the better fuelling efficiency resulting from the change of recycling properties around the LID head.

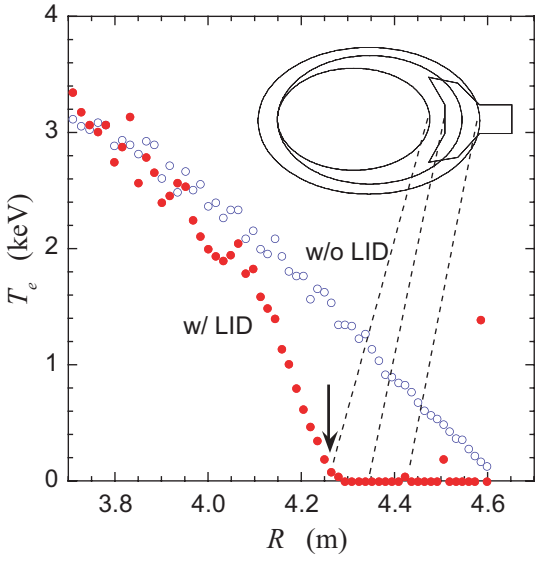

Fig. 3. Radial profiles of electron temperature for the plasma with helical divertor configuration (open circles) and LID configuration (closed circles) in LHD.

Control of radial electric field

Changing the magnitude and radial profiles of the helical ripples is be the most straightforward tool for controlling the radial electric field. The reason is that the radial electric field in LHD is determined by the ambipolar condition of the ion flux and electron flux that are trapped in helical ripples. In LHD, the radial profiles of the helical ripples

can be controlled by shifting the magnetic axis from 3.9 m to 3.5 m. The radial profiles of radial electric field are measured with charge-exchange spectroscopy using the charge-exchange reaction between the neutral beam and a fully stripped impurity. The measurements are restricted to the region where the line of sight crosses the neutral beam (R = 3.8–4.2 m). Therefore, the radial electric field is obtained for the whole plasma when the magnetic axis is shifted outward (R_{ax} = 3.9 m), while only half the plasma minor radius can be covered for the plasma when the magnetic axis is shifted inward (R_{ax} = 3.5 m).

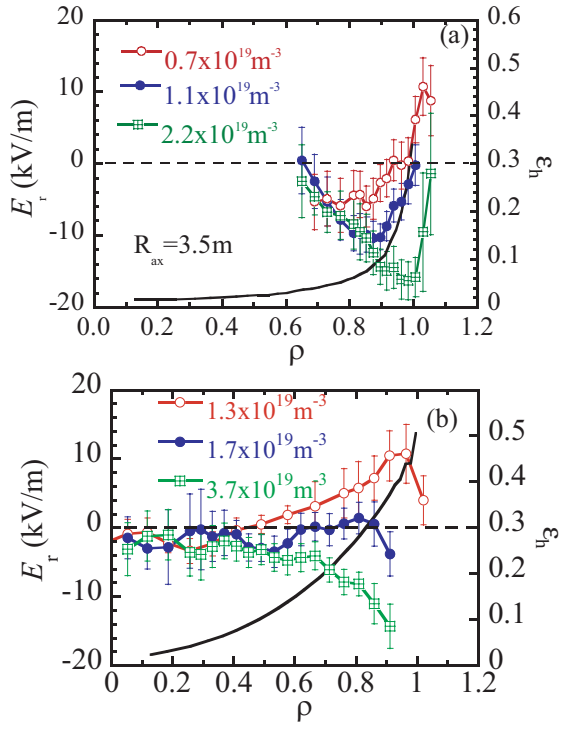

Fig. 4. Radial profiles of radial electric field for three different densities for a magnetic axis of (a) 3.5 m (inward-shifted configuration) with γ = 1.254 and (b) 3.9 m (outward-shifted configuration) with γ = 1.254. The radial profiles of effective helical ripple, ε_h, are plotted as solid lines.

Figure 4 shows the radial profiles of the radial electric field for the ion root (large neoclassical flux with negative E_r in the high collisionality regime), the electron root (small neoclassical flux with positive E_r in the low collisionality regime), and the transition regime (between the ion root and the electron root) for various configurations with different helical ripple profiles. When the helical ripple increases gradually towards the plasma edge (R_{ax} = 3.9 m), the electron root region can be extended to half the plasma minor radius and the radial electric field shear that is produced is relatively weak in a plasma with lower electron density. However, when the helical ripple increases sharply at the plasma edge (R_{ax} = 3.5 m), the electron root region can be localized at the plasma edge and strong radial electric field shear is produced in plasmas with lower electron density.

High ion temperature

At present, LHD has three 180-keV tangential neutral beam lines that use negative ion-sources in order to be efficient at these energies. They are effective tools for the experiment, but contribute primarily to electron heating rather than ion heating. To increase the ion temperature to 10 keV and to investigate the properties of high-ion-temperature plasmas, experiments using high-Z plasmas have been carried out with Ar and/or Ne as fuelling to increase beam absorption and energy deposition to ions in low-density plasmas. Intensive Ne and/or Ar glow discharge cleaning is applied to reduce the wall-absorbed hydrogen and increase the concentration of Ne and/or Ar ions. As a result, the ion temperature increases with an increase in the ion heating power normalized by the ion density, and the highest ion temperature obtained in LHD has increased from 5 keV to 13.5 keV in the last three years. However, plasmas with large concentrations of high-Z impurity are not relevant for nuclear fusion research because of the large dilution of the fuel. Therefore, this is intended as a preparatory experiment to study the property of high-ion-temperature plasmas up to 10 keV and to demonstrate the capability of LHD as a magnetic confinement device, before the installation of a low-energy (40-keV) neutral beam for ion heating (which is planned in the near future). The ion temperature increases with increasing normalized ion heating power in plasmas with Ar and Ne puffing as shown in Fig. 5. No distinct saturation has been observed.

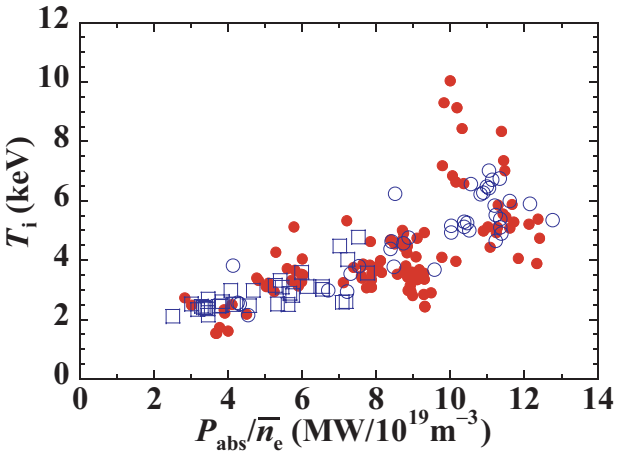

Fig. 5. Ion temperature as a function of the direct ion heating power normalized by the ion density in the plasma with Ar puff (circles) and Ne puff (squares) for plasmas with a magnetic axis of 3.6 m (open symbols) and 3.7 m (closed symbols).

Particle transport

Hollow density profiles are often observed in LHD, in contrast to the peaked density profiles observed in tokamak plasmas. A hollow profile even in the steady state suggests outward convective velocity in the core region, because density profiles should be flat during steady state in a plasma in which most of the particle source is localized at the plasma edge. In order to study the parameter dependence of diffusion and convective velocity in the plasma, a modulated gas puff is applied to the plasma.

The diffusion coefficient D increases as the temperature is increased, as seen in Fig. 6. The temperature dependence of the diffusion coefficient is $T_e^{1.7 \pm 0.9}$ in the core ($\rho < 0.7$) and $T_e^{1.1 \pm 0.14}$ in the edge ($\rho > 0.7$). Both values are close to that expected from gyro-Bohm scaling, $T_e^{1.5}$. The dependence of edge diffusion on the magnetic field is measured to be B^{-2}, which is also consistent with the prediction of gyro-Bohm scaling. The fluctuation characteristics are also studied using CO_2 laser scattering. In general, the diffusion coefficient is proportional to the frequency width and inverse of the wave number of the fluctuations, as well as the fluctuation amplitude. A decrease in the peak wave number and a broadening of the frequency spectrum of fluctuations are observed as the heating power is increased. These changes of the fluctuation spectrum are qualitatively consistent with enhanced diffusion at higher heating power.

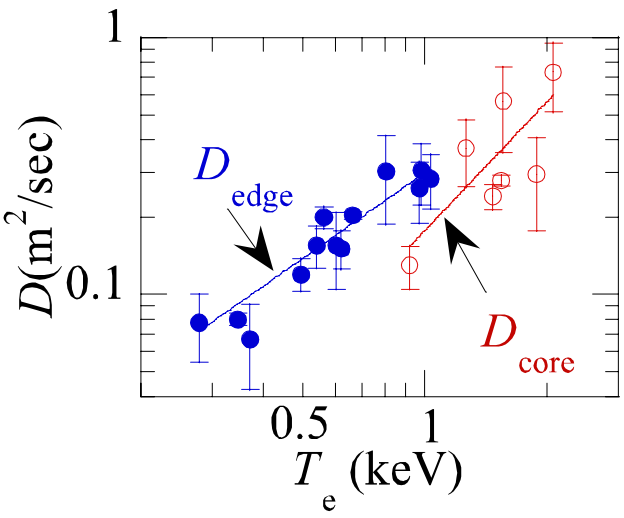

Fig. 6. Electron temperature dependence of the diffusion coefficient.

Electron transport

An electron ITB is characterized by the peaked electron temperature profile associated with the transition from the ion root to the electron root observed in NBI-sustained plasmas with centrally focused ECH. The characteristics of the formation of the ITB depend on the direction of the neutral beam. Figure 7 shows the increment of the electron temperature ΔT_e at the plasma center due to ECH power as a function of ECH power normalized by the electron density. The threshold power for the transition to the ITB plasma is clearly observed in plasmas with counter (CNTR) NBI in the direction that the beam-driven current decreases the rotational transform in the plasma. This is in contrast to the fact that the central T_e increases almost linearly with ECH power and no clear threshold power for the transition to ITB plasma is observed in plasmas with co (CO) NBI in the direction of increasing rotational transform by beam-driven current. The differences in the characteristics are due to differences in rotational transform ι and not to differences in the deposition profile. In plasmas with CNTR NBI, the rational surface of $\iota = 1/2$ is located at half of the plasma minor radius, while the plasma with CO NBI has no $\iota = 1/2$ rational surface because of the increase of central rotational transform above 0.5 in plasmas with an inward-shifted configuration ($R_{ax} < 3.6$ m). As the magnetic axis shifts outward ($R_{ax} > 3.75$ m), the rational surface of $\iota = 1/2$ moves toward the plasma edge and always exists in the plasma, regardless of the direction of the NBI. Thus the difference in characteristics of the ITB between CO NBI and CNTR NBI becomes small.

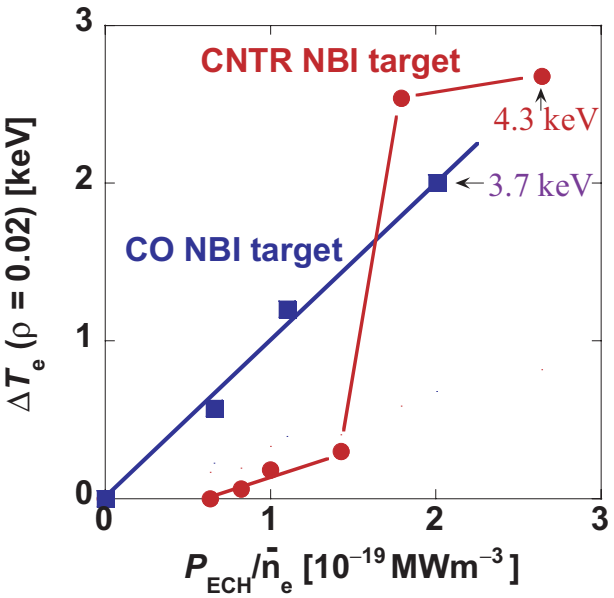

Fig. 7. Electron temperature increases at the center and periphery are plotted as a function of density-normalized ECH power.

Summary

In the inward-shifted configuration where the beta limit is expected to be low (1.5% in the Mercier limit), a high beta plasma with $\langle \beta_{dia} \rangle = 4.3\%$ is obtained in the high-aspect-ratio configuration where the pitch parameter of the helical coil γ is 1.20. The beta values achieved significantly exceed the linear MHD stability criteria and the Mercier limit and reached the region where the low-n (m/n =1/1) ideal MHD modes are predicted to be unstable. A heliotron plasma exhibits negative shear and a magnetic hill, in contrast to a tokamak plasma's positive shear and magnetic well. Negative magnetic shear is thought to contribute to the formation of an electron ITB. The electron ITB is observed in a tokamak when the magnetic shear changes its sign from positive to negative. In a heliotron plasma, where the magnetic field shear is negative, the electron ITB is usually observed with ECH heating in the electron root.

The LID is now showing good capability as a powerful tool for edge control to achieve an improved confinement regime. It is an important element of the LHD project. The LHD plays a key role as a three-dimensional currentless steady-state magnetic confinement device that will supply a high-quality database for the plasma physics and sciences necessary to realize controlled nuclear fusion. Further work should be focused on (1) steady-state physics, (2) high-beta physics, and (3) confinement improvement and edge control.

Akio Komori and LHD experimental group
National Institute for Fusion Science
Toki 509-5292, Gifu, Japan

E-mail: komori@LHD.nifs.ac.jp

Extended abstracts

Fast recovery of vacuum magnetic configurations of W7-X stellarator using function parametrization and artificial neural networks

Nucl. Fusion **44** (2004)1176

Methods of fast recovery of the vacuum magnetic configuration of Wendelstein 7-X (W7-X) stellarator, under construction at IPP-Greifswald (Germany), are reported. In this study the projected typical configuration space was covered by a database of 1210 vacuum configurations and statistically analyzed. The dependent parameters to be recovered were expressed as quadratic or cubic polynomials in terms of the coil current ratios. These parameters comprise the magnetic axis positions, the magnetic field axis values, and the profiles of iota and the specific volume. The detectable major magnetic island chains (5/5, 5/6) were modeled in the form of their locations $r_{\mathrm{eff}}^{(\mathrm{is})}$ and width $w^{(\mathrm{is})}$. The 5/4 islands were omitted from the analysis because ergodic regions around what is left of the island prohibited a consistent analysis.

The standard quadratic function parameterization (FP) model was found to be insufficient for an accurate recovery of the axis parameters, and failed completely for parameters connected with the boundary (separatrix). The cubic FP (c-FP) model, involving trebling of the model size, improved the quality of recovery significantly. In case of the island parameters, changing the regression from $r_{\mathrm{eff}}^{(\mathrm{is})}$ and $w^{(\mathrm{is})}$ to $[r_{\mathrm{eff}}^{(\mathrm{is})}]^2$ and $[w^{(\mathrm{is})}]^2$ proved crucial to improving the recovery of these parameters. This was checked in a one-dimensional study, in which a sequence of magnetic configurations with an island chain was generated by varying only one coil current (Fig. 1). An interesting aspect was the performance of the artificial neural network (ANN) model, incorporating a nonlinear sigmoidal function, which performed almost as well as the c- FP model for the scalar parameters and outperformed it for a few of the axis parameters. The study also included an investigation of errors in the coil current measurements. For an error of up to 0.1% of a coil current of 12 kA (three times the designed level for W7-X), the c-FP model was able to keep the recovery errors within acceptable limits. In an inverse transformation, the coil current ratios were very well recovered by a c-FP model in terms of physical properties of the configuration. Here, the ANN model had to be Principal-Component-Transformation-based, with a preprocessed set of inputs, to perform almost as well as the c-FP model.

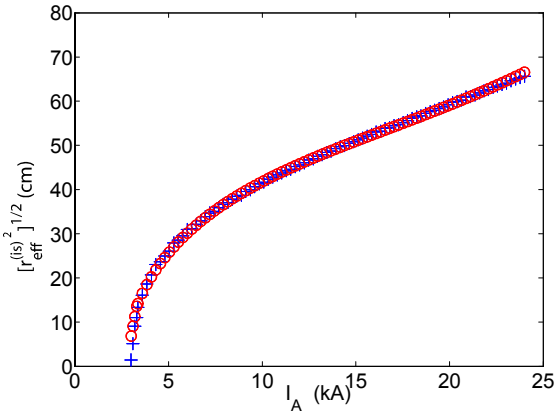

Fig. 1. Variation of $|r_{eff}^{(is)}|$ with IA. Crosses (+) indicate observed data; open circles (o) a c-FP fit. The obvious parabolic behavior explains the use of $[r_{eff}^{(is)}]^2$, rather than $r_{eff}^{(is)}$, as the regressed variable.

Joachim Geiger
Max-Planck-Institut für Plasmaphysik
IPP-EURATOM Association
D-17489 Greifswald, Germany
E-mail: joachim.geiger@ipp.mpg.de

Novel mechanism of anomalous electron heat conductivity and thermal crashes during Alfvénic activity in Wendelstein 7-AS

Experiments on the stellarator Wendelstein 7-AS (W7-AS) have shown that bursts of Alfvénic activity associated with the injected ions can lead to strong drops (up to 30%) of the plasma energy content, the plasma temperature being mainly affected. This motivated the present work, in which a theory of the influence of a monochromatic Alfvén wave on the electron transport is suggested and a particular shot in W7-AS is analyzed in detail. It follows from our theory that the presence of kinetic Alfvén waves (KAW) can strongly enhance the electron heat flux, especially in the regime of strong collisions (when the collision frequency exceeds the bounce frequency of thermal electrons in the wave field). This mechanism may be of importance for both laboratory and space plasmas. It can be responsible for strong drops of the plasma energy without noticeable density variations in the W7-AS shot 34723 (Fig. 2). The considered mechanism is typically less effective in tokamak plasmas, where the regime of strong collisions does not take place. This explains why large thermal crashes have not been observed in tokamaks.

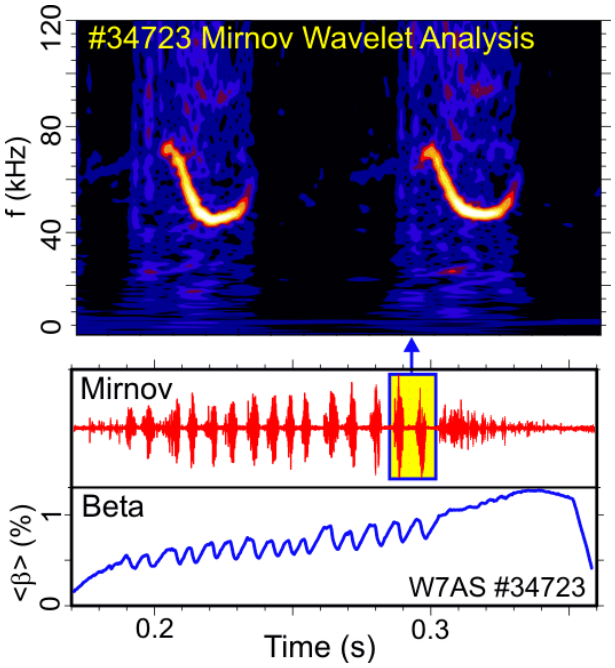

Fig. 2. Discharge at 1.25 T showing repetitive bursts of Alfvén eigenmodes with strong frequency sweeping and large effect on the thermal confinement during the density ramp-up phase.

Ya. I. Kolesnichenko,[1] Yu. V. Yakovenko,[1] A. Weller,[2] A. Werner,[2] J. Geiger,[2] V. V. Lutsenko,[1] and S. Zegenhagen[2]
[1]Institute for Nuclear Research
Prospekt Nauky 47
Kyiv 3680
Ukraine
[2]Max-Planck-Institut für Plasmaphysik
IPP-EURATOM Association
D-17489 Greifswald, Germany

Active probe experiments at the Wendelstein 7-AS stellarator

Submitted to Plasma Physics and Controlled Fusion

Fluctuations in the edge plasma of magnetic fusion experiments play an important role in terms of anomalous energy and particle transport. Experiments on Wendelstein 7-AS were conducted to investigate the propagation of actively fed signals driven by electrical probes. The goal of these investigations is an improved understanding of the turbulence and potentially a method to tailor the edge plasma turbulence. Two movable poloidal probe arrays were used for the experiments, one located on the inboard side of the vessel and the other on the outboard side. A subset of probe tips was used for actively driving the plasma by different control signals; the remaining probes collected fluctuation data in the plasma boundary. With this set-up it was possible to investigate the signal propagation in the poloidal direction and also parallel to the magnetic field. Poloidally, we find a significant cross-correlation between active and passive probes. From analysis of the cross-coherency and phases of the signal with passive probe tips, a dominant influence of the background plasma rotation on the applied signals is observed, as shown in Fig 3. In the case of waves driven by several phase-locked active probes, the direction of the wave propagation with respect to the plasma rotation (co- or counter-rotating) is essential for an effective coupling to the turbulent plasma. Also, the signal propagation parallel to the magnetic field depends on co- or counter-rotation with respect to the background plasma rotation. The parallel phase velocity was found to be compatible with the electron thermal velocity.

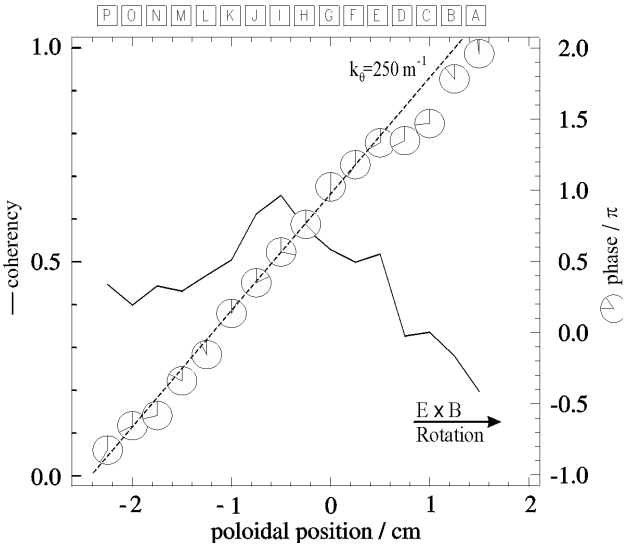

Fig. 3. The coherency (solid lines) and phase (clocks) at a frequency of 60 kHz versus the poloidal position given by the probe tips of the detection probe array. The reference for the lock-in analysis is the 60-kHz sine signal fed into the plasma at the distant exciter probe tip (12 m parallel to the magnetic field). The highest coherency is observed at the tip (I) of the array. The maximum parallel phase velocity of the signal can be estimated from the phase shift.

Henning Thomsen
Max-Planck-Institut für Plasmaphysik
IPP-EURATOM Association
D-17489 Greifswald, Germany
E-mail: henning.thomsen@ipp.mpg.de